Advanced Journal of Chemistry, Section A, 2024, 7(2), 110-121

Advanced Journal of Chemistry, Section A

journal homepage: www.ajchem-a.com

Original Research Article

Impact of Annealing Temperature on Hydrothermally Synthesized Copper Antimony Oxide (Cu_2Sb_2O) from Amorphous Phase to Monoclinic Structure

Imtiaz Ahmad[1, 2], Javaria Razzaq[1, 3], Ammara Ammara[1, 4], Ferhan Kaleem[1, 5], Muhammad Qamar[1, 4], Shahid Ilahi[1, 5], Imosobomeh Lucky Ikhioya[1, 6]*

[1] *National Centre for Physics, Quaid-i-Azam University Campus, Islamabad, Pakistan*
[2] *Department of Physics, University of Engineering and Technology, Lahore, Pakistan*
[3] *Department of Physics, University of Agriculture Faisalabad, Pakistan*
[4] *Department of Physics, Ripah International University Islamabad, Faislabad Campus, Pakistan*
[5] *Institute of Chemical Sciences Bahauddin Zakariya University Multan, Pakistan*
[6] *Department of Physics and Astronomy, University of Nigeria, Nsukka, Nigeria*

ARTICLE INFO

Article history

Submitted: 05 October 2023
Revised: 17 October 2023
Accepted: 13 November 2023
Available online: 14 November 2023

Manuscript ID: AJCA-2310-1429
Checked for Plagiarism: **Yes**
Language editor:
Dr. Fatimah Ramezani
Editor who approved publication:
Dr. Hoda Hamidi

DOI: **10.48309/ajca.2024.419363.1429**

KEYWORDS

Copper
Antimony
Hydrothermal
Amorphous
Monoclinic structure

ABSTRACT

In this study, a hydrothermal approach has been employed for the synthesis of copper antimony oxide films. Cu_2Sb_2O exhibits an amorphous phase prior to annealing and a polycrystalline phase (monoclinic structure) after annealing at temperatures ranging from 200 to 400°C, as showed by the XRD. The angles of 26.934°, 34.228°, and 38.362° correspond to the diffraction peaks (111), (211), and (311). High annealing temperature caused the film's lattice to reform and crystalize, which could cause cell ignition. The diffraction angles of the peaks moved higher because it was assumed that the annealing process affected the material. The unannealed Cu_2Sb_2O material displays small nanoparticles and a noteworthy nanoflake structure. Under different annealing temperatures, the nanoparticle's size increases when the film surface is ignited at higher pressure. When nanoparticle clusters were present during annealing, the material's surface energy increased. The absorption spectra displayed a consistent high rate of absorption between 200 to 600 nm, but showed a considerable decline beyond this range, with the minimum point noted between 700 to 850 nm. Yet it increased again between 980 and 1100 nm wavelength range. Light absorption is high in Cu_2Sb_2O, specifically in ultraviolet and blue regions. The film's absorbance increased from 0.145 to 0.185 a.u. when Cu_2Sb_2O was annealed at 200 °C. An increase in temperature from 200 to 400 °C caused an improvement in Cu_2Sb_2O's absorbance because of its susceptibility to temperature. The low reflectance of the films in both areas makes them ideal for both solar and photovoltaic cells. As the annealing temperature increased from 200 to 400 °C, the synthesized Cu_2Sb_2O film's bandgap energy decreased from 1.78 eV to a range of 1.66–1.21 eV.

GRAPHICAL ABSTRACT

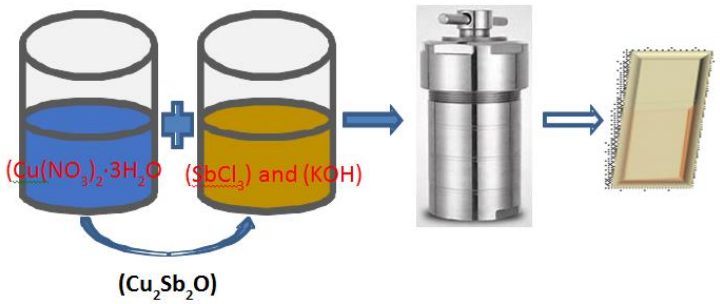

* Corresponding author: Ikhioya, Imosobomeh L.
✉ E-mail: imosobomeh.ikhioya@unn.edu.ng

Introduction

Chalcogenides semiconductors are under study for potential use in technological, thermoelectric, infrared materials, and optoelectronic applications. Chalcogenide materials have many useful properties and are used in many applications because they are abundant, cheap, and environmentally friendly [1–15]. These materials are now crucial for optoelectronic and optical applications [4, 12].

Among the absorber materials for 3D film solar cells, CuSbO's p-i-n structure may be the most photovoltaic, with a high coefficient and band gap of 1.5 eV, which is close to the optimal range for photovoltaic conversion [6,7]. Despite the existence of many thin film types, ternary oxide thin films have garnered significant interest for their distinctive ability to transmit and absorb visible light [5]. They possess moderate energy band gaps, which are often credited for their remarkable charge transport properties. Researchers have created various TMO materials to broaden the use of lithium-ion batteries [3].

Phetcharat Chongngam *et al*. [16] achieved the successful synthesis of Cu_2Sb thin films through chemical bath deposition method. Annealing of the thin film is carried out at 300, 400, and 500 °C. The X-ray diffraction outcomes for the Cu_2Sb thin films displayed the $CuSb_2O_6$ phase for the films prepared at 300 ˚C, 400 ˚C, and the as-prepared films, demonstrating crystal formation.

The thin film became amorphous after being annealed at 500 ˚C. Field-emission scanning electron microscopy was utilized to analyze surface morphologies. The properties assessed included linear optical, dispersion, optoelectrical, and nonlinear optical. The electrical properties, energy bandgap, and Urbach energy were determined. Optimal results can be achieved for synthesized mixed-phase thin films by avoiding annealing above 400 ˚C. Eventually, the Cu_2Sb thin film showed majority carrier conductivity of the P-type. The unique qualities of thin-film substances could be useful in optoelectronics, nonlinear optics, and as an absorbing layer for solar cells.

There are various methods to synthesize nanomaterials. The hydrothermal method is essential for synthesizing thin films, according to Pawar and Deshmukh [17].

The hydrothermal method, a heterogeneous reaction, is carried out using the autoclave. Place insoluble solutes into the autoclave and keep it in the oven at a temperature below the supercritical point of water. Thin films with different shapes and sizes of crystallization have formed on the substrate. Water is the preferred solvent throughout the reaction. Different temperature and pressure reveal remarkable properties. Non-polar compounds fully dissolve in water due to its high density. By adjusting process parameters, this method can create various structures, including three-dimensional nonospheres, two-dimensional nanosheets, and one-dimensional nanowires. These structures have uniform shapes and consistent composition [4].

This method is mainly used to dissolve insoluble materials at high temperature and pressure. Advanced methods for preparing nanostructures require expensive instruments and surfactants. These method generates a byproduct that harms the environment. Pawar and Deshmukh [17] suggests that the hydrothermal method is eco-friendly as it uses low temperatures and doesn't require harmful catalysts. This technique helps control material shape and makes sure coatings stick well to various surfaces.

In this study, copper-antimony oxide (Cu_2Sb_2O) was synthesized using the hydrothermal method. Our research suggests that Cu_2Sb_2O has promising physical properties, making it suitable for photovoltaic and optoelectronic applications. The study aimed to examine the impact of Cu_2Sb_2O on structural, morphological, optical, and electrical properties using hydrothermal methods. It also explored the potential of thin-

film synthesis for practical optoelectronic applications and sought to identify a new absorber layer for use in solar cell technology.

Details experimental

Materials

The materials used in this study are copper nitrate trihydrate ($Cu(NO_3)_2{\cdot}3H_2O$) Sigma-Aldrich 99.9%, Antimony chloride ($SbCl_3$) Sigma-Aldrich 99.9%, potassium hydroxide (KOH), polyethylene glycol, α-terpineol, deionized water, heating mantle, FTO-fluorine-doped tin oxide substrate, an oven that has a temperature range of 50 to 1000 °C.

Synthesis of the copper antimony oxide (Cu_2Sb_2O)

We added a 0.2 M solution of copper nitrate trihydrate ($Cu(NO_3)_2{\cdot}3H_2O$) from Sigma-Aldrich, which was 99.0% pure, to 30 mL of deionized water and stirred it for 40 minutes at room temperature. Antimony chloride ($SbCl_3$) and potassium hydroxide (KOH) were dissolved in deionized water in equimolar amounts and stirred for 40 minutes. Gradually, the solution of antimony chloride and potassium hydroxide were added to the solution of copper nitrate trihydrate. 1 g of polyethylene glycol and 1 g of α-terpineol were added as well, before stirring for 40 minutes at room temperature to make a uniform solution.

To undergo hydrothermal processing, the FTO glass and solution were placed in a 100 mL Teflon-lined, stainless-steel autoclave. The temperature of the solution was kept constant at 200 °C for 6 hours. As the autoclave cooled down to room temperature naturally, the deposited Cu_2Sb_2O on FTO substrate was vacuum-dried at 60 °C for 40 minutes. To analyze the effect of annealing temperature on Cu_2Sb_2O films, three samples were annealed at temperatures of 200, 300, and 400 °C for 2 hours each. The samples were analyze for their optical, electrical, structure, morphology, and elemental compositions using various characterization technique. The NPUFEI-NNS45 SEM was employed for the analysis of structural and elemental compositions. The JASCO-FTIR (FT/IR-6600) was used to examine the presence and types of functional groups in the Cu_2Sb_2O films. The absorbance wavelength of the films was obtained using a 756S UV-Visible spectrophotometer within the optical spectral range of 300 to 110nm. The electrical properties of the films were analyzed using the Jandel four-point probes method.

Discussion of results

XRD study of Cu_2Sb_2O

Figure 1 shows the XRD pattern of the thin film material of copper antimony oxide (Cu_2Sb_2O). The pattern shows Cu_2Sb_2O in an irregular phase before annealing and in a polycrystalline phase (monoclinic structure) after annealing at different temperatures between 200 and 400 °C. The diffraction peaks (111), (211), and (311) correspond to 2theta angles of 26.934°, 34.228°, and 38.362° respectively. The crystallization of the synthesized material is evident from the most prominent (111) diffraction peak. The film's lattice reformed and crystallized because of high annealing temperature, which may cause cell ignition. The assumption is that the annealing process caused an effect on the material, resulting in the peaks shifting to higher diffraction angles.

Heat treatment facilitates recrystallization of the material. The ions Sb^{3+} are oxidized, leading to the formation of Sb^{5+} ions. The smaller ionic radius of Sb^{5+} ions compared to Cu^{2+} ions allows them to replace Cu^{2+} ions on the lattice, leading to a decrease in the unit cell volume in the lattice. The higher annealing temperature over 200°C was caused by the saturation of Sb^{5+} incorporation leading to an increase in lattice expansion. As a result, the energy required for

defect creation increased and the peak shifted to higher diffraction angles [16, 18, 19]. The crystallite size of Cu_2Sb_2O in Table 1 decreases with higher annealing temperatures. The modest shift in peak locations could be caused by the annealing temperature. The annealing temperatures of 200, 300, and 400 ˚C yielded crystallite sizes of 1.843, 1.832, and 1.821 nm, respectively. Using equations (1-5) [20-35], calculations were performed to determine different structural characteristics such as FWHM, D, d, lattice constants, and dislocation density.

$$D = k\lambda/\beta \cos\theta \quad (1)$$

$$d = \lambda/2 \sin\theta \quad (2)$$

$$a = \sqrt{c^2/3} \quad (3)$$

$$c = {}^{\lambda}/_{sin\theta} \quad (4)$$

$$\delta = 1/D^2 \quad (5)$$

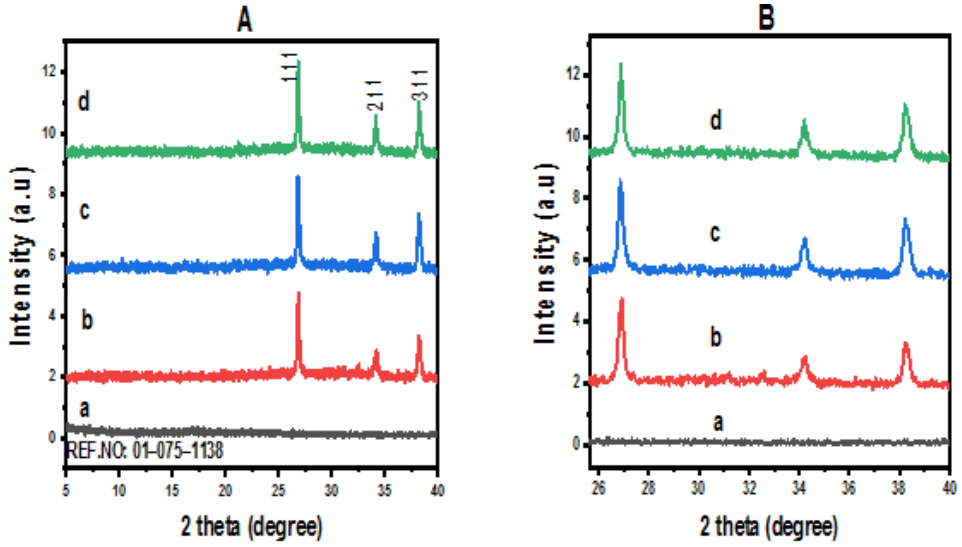

Figure 1. XRD pattern (A) and magnified version (B) of unannealed Cu_2Sb_2O-(a), annealed at 200 ˚C-(b), annealed at 300 ˚C-(c), and annealed at 400°C-(d).

Table 1. structural properties of Cu_2Sb_2O

Films	2θ (deg.)	d (spacing) Å	a (Å)	(β)	(hkl)	(D) nm	σ lines/m² X 10¹⁸
Cu_2Sb_2O unannealed	26.450	3.369	5.835	1.578	011	0.893	3.731
	-	-	-	-	-	-	-
	-	-	-	-	-	-	-
Cu_2Sb_2O 200 ˚C	26.934	3.309	5.732	0.7654	111	1.843	8.765
	34.228	2.619	5.238	0.7662	211	1.855	8.483
	38.362	2.346	4.692	0.7668	311	1.832	8.297
Cu_2Sb_2O 300 ˚C	26.934	3.309	5.732	0.7698	111	1.832	8.866
	34.228	2.619	5.238	0.7721	211	1.841	8.614
	38.362	2.346	4.692	0.7732	311	1.817	8.437
Cu_2Sb_2O 400 ˚C	26.934	3.309	5.732	0.7745	111	1.821	8.975
	34.228	2.619	5.238	0.7747	211	1.834	8.672
	38.362	2.346	4.692	0.7749	311	1.813	8.474

Where D is the crystallite size, λ is the wavelength, β is the full width at half maximum, d is the d-spacing, a is the lattice constant, δ is the dislocation density**.** Table 1 shows that there is a correlation between the decrease in average crystallite size and the strain induced during annealing. This is confirmed by the 2theta angles. The synthesis process might have caused the strain because of the nucleation process. Research has showed that when the angle increases, there is a significant change in the distances between planes and the density of dislocations.

Surface morphological analysis of Cu_2Sb_2O films

Figure 2 displays the surface morphology of Cu_2Sb_2O. Small nanoparticles and a significant nanoflake structure are evident in the unannealed Cu_2Sb_2O material. The size of the nanoparticle increases when the film surface is ignited with higher pressure upon annealing at different temperatures. The presence of nanoparticle clusters during annealing resulted in an increase in the material's surface energy. High-temperature caused strains that made the nanoparticle more susceptible to agglomeration. A change in orientation of the lattice occurred due to the strain, which caused a dislocation to form near the surface. The lattice strain corresponds with the observed strain in their structural property. The elemental composition of Cu_2Sb_2O is shown in Figure 3. The spectrum shows all the elements necessary to form Cu_2Sb_2O. The other element observed could be the composition of the FTO substrate used during synthesis.

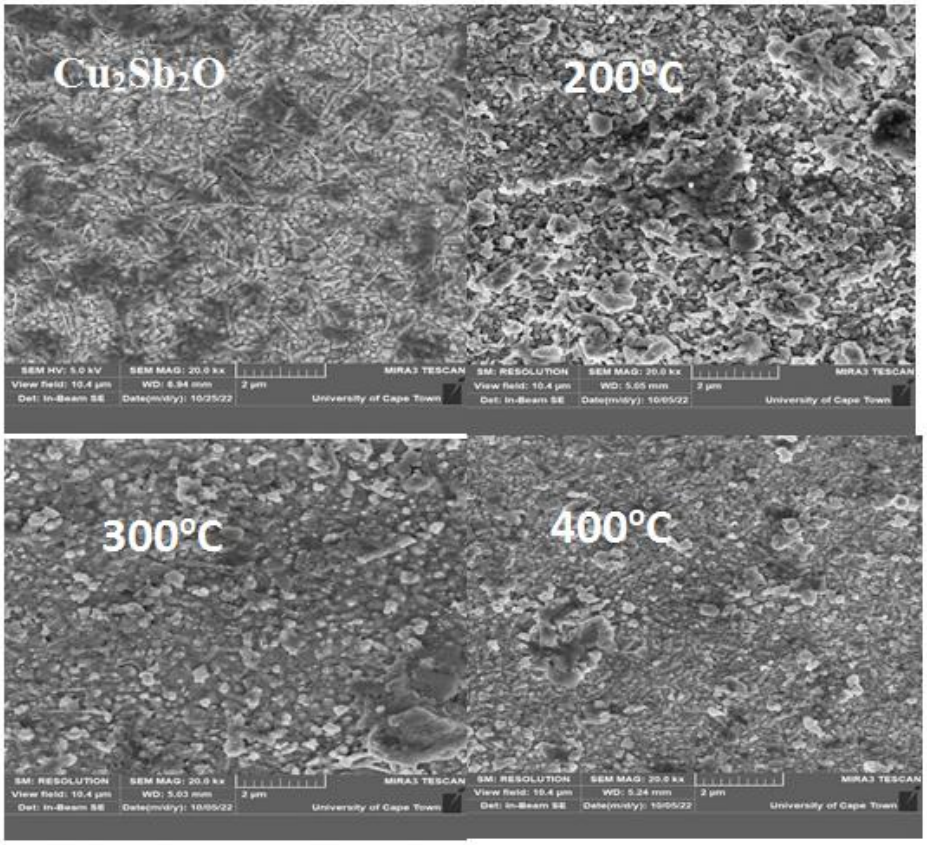

Figure 2. SEM of Cu_2Sb_2O.

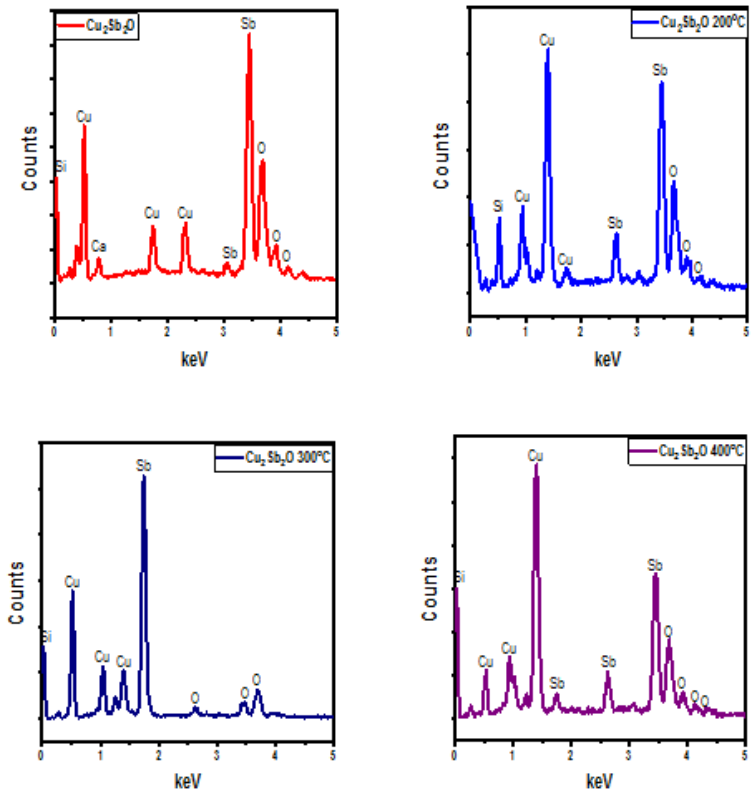

Figure 3. EDXs of Cu_2Sb_2O.

Optical study of Cu_2Sb_2O

Figure 4 (J1) was analyzed in a study to measure the absorbance level of Cu_2Sb_2O. Absorption spectra maintained a high rate of absorption from 200 to 600 nm but decreased significantly beyond that point, with the lowest point at 700 to 850 nm. However, it rose once more during the wavelength range of 980 to 1100 nm. Cu_2Sb_2O has a high capacity for absorbing light, especially in the ultraviolet and blue regions. Annealing Cu_2Sb_2O at 200 ˚C improved the film's absorbance from 0.145 to 0.185 a.u. Raising the temperature from 200 to 400 ˚C improved Cu_2Sb_2O's absorbance due to its sensitivity to temperature. The absorbance went up from 0.185 to 0.610 a.u. The increase in absorbance is caused by the annealing temperature's effect on Cu_2Sb_2O. The increase in crystallite peak seen in the XRD pattern may be linked to the growth in crystallite size after annealing. An increase in the size of the crystallite can cause an increase in the specific surface area and consequently lead to a higher optical absorbance [25-35]. The films are good for solar cell technology, energy production, and photovoltaic applications because they absorb a lot. At a wavelength of 1100 nm, the rate of transmittance in Figure 4 (J2) was consistently high, even reaching 100%. The spectral region of infrared shows high transmittance for Cu_2Sb_2O. There is a rise in the transmittance spectra as the annealing temperature decreases from 400 to 200 ˚C. The films showed a decrease in electrical resistivity which could be the reason. Optical transmittance may improve if specific surface area is increased by reducing film thickness [25-30]. Due to their high transmittance rate, these films are a perfect fit for photovoltaic uses, energy production and solar cell systems. In Figure 4 (J3), the highest reflectance was detected in the UV region. For both annealed and unannealed Cu_2Sb_2O at 200 ˚C, the film displayed less than 10% reflectance in the visible,

ultraviolet, and infrared regions, except for a reflectance of 20% in the ultraviolet region. The films were found to have low reflectance in both regions, making them highly suitable for use in both solar and photovoltaic cells. The graph of $(\alpha hv)^2$ Vs hv is used to represent the energy bandgap of Cu_2Sb_2O in Figure 4 (J4). By utilizing the graph, which depicted the absorption coefficient square and photon energy, the indirect bandgap of the produced films was established. The indirect bandgap energy of the synthesized Cu_2Sb_2O film decreased from 1.78 eV to a range of 1.66–1.21 eV as the annealing temperature increased from 200 to 400 °C.

As depicted in Figure 5 (J5), the refractive index of Cu_2Sb_2O films has been illustrated. The transmission of light frequency from 1.0-4.0 eV shows a considerable increase as the annealing temperature is raised from 200 to 400 °C, despite a sharp decline at 2.6 eV. As the energy level increases, the refractive index of the films also rises. The highest peaks of the refractive index were identified to be located in the energy range of 2.65 eV. The increase in refractive index due to annealing temperature is the reason why these materials are a perfect match for solar and photovoltaic cells. Figure 5 (J6) shows that the extinction coefficient of Cu_2Sb_2O films increases with an increase in annealing temperature from 200 to 400 °C, and the photon energy of the material also rises, as observed from the presented results. From the data presented in Figure 5 (J7), it is clear that the Cu_2Sb_2O films demonstrate an increase in optical conductivity as the photon energy increases, and furthermore, the annealing process serves to stabilize both the electrical and optical conductivity of the films.

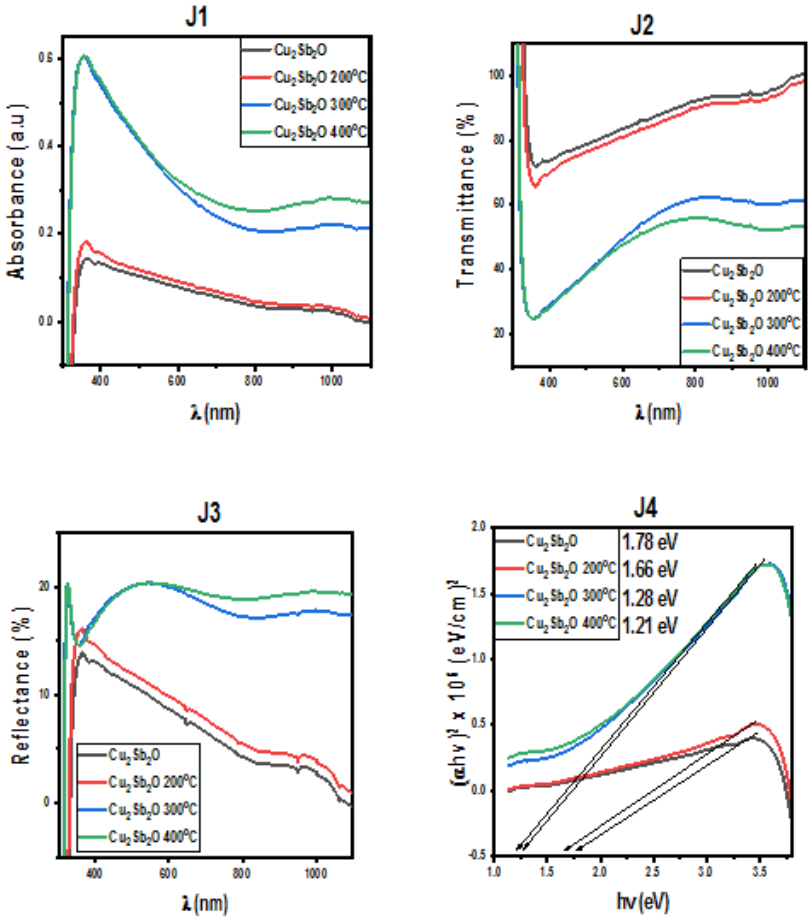

Figure 4. UV plots of Cu_2Sb_2O absorbance (J1), transmittance (J2), reflectance (J3), and bandgap energy (J4).

The real dielectric constant (RDC) of Cu_2Sb_2O films is depicted in Figure 6 (J8). As the annealing process progresses, the RDC (relative dielectric constant) tends to increase with the photon energy, ranging from 1.0-4.0 eV, but experiences a sudden drop at 2.65 eV. The rise of RDC films is directly proportional to the increase in energy. In our observation, we were able to identify the highest peaks of RDC specifically within the energy range of 3.85 eV. By increasing the annealing temperature, it is possible to make RDC suitable for solar and photovoltaic cells. The data presented in Figure 6 (J9) demonstrates that there is a positive correlation between IDC and photon energy, and there is a further increase in IDC when films undergo annealing.

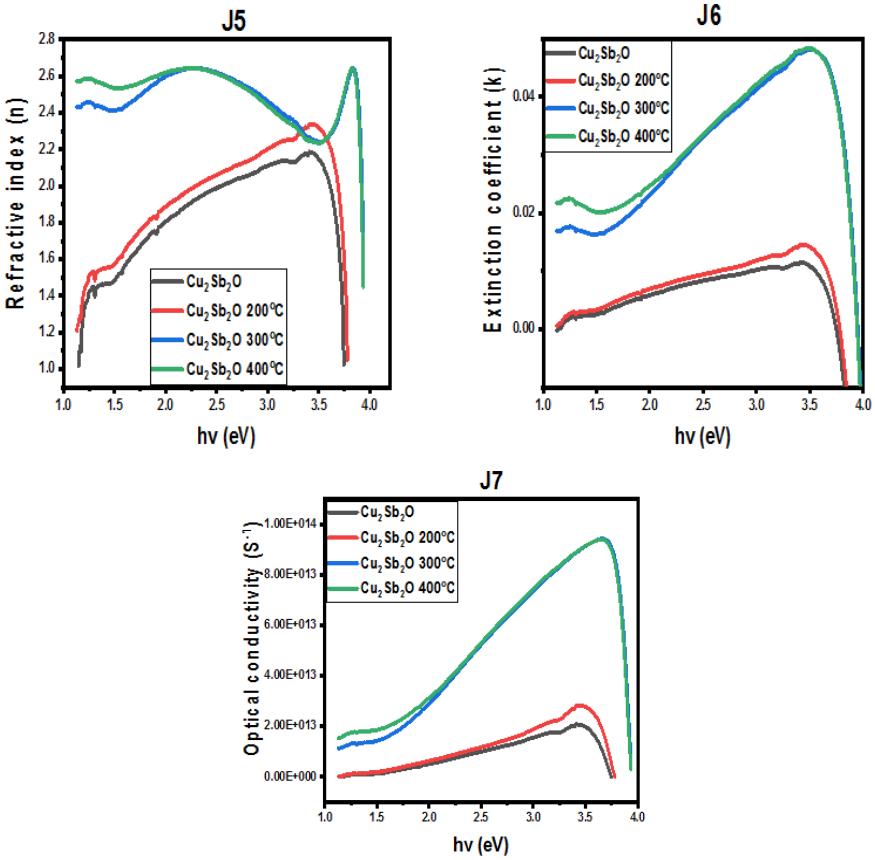

Figure 5. UV plots of Cu_2Sb_2O refractive index (J5), extinction coefficient (J6), and optical conductivity (J7).

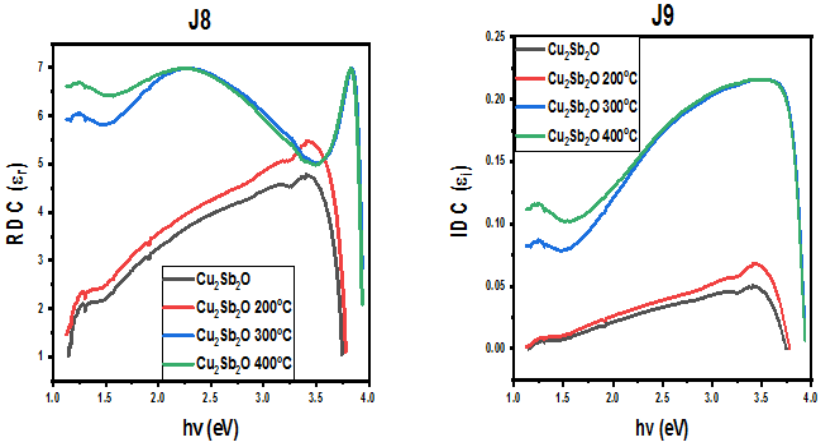

Figure 6. UV plots of Cu_2Sb_2O real (J8) and imaginary dielectric constant (J9).

Electrical study

Figure 7 demonstrates the correlation between film thickness and electrical resistivity or conductivity. A decrease in material thickness results in an increase in electrical conductivity and a corresponding decrease in resistivity. The alignment is due to the fact that carrier concentration is increased by annealing temperature, which enhances electrical conductivity. The ability of the material to handle more electric current is beneficial for optoelectronic applications. Table 2 presents the analysis of resistivity and conductivity for Cu_2Sb_2O, offering valuable insights into its electrical properties. The electrical conductivity of the film increased from 3.88 to 6.01 (S/m) as its thickness declined from 117.53 to 105.31 nm due to annealing temperature and its resistivity decreased from 25.77 to 16.62 (Ω.cm). The electron-hole pairs in Cu_2Sb_2O are affected by the annealing temperature, which is linked to the crystallite size and results in increased space between them. Annealing process results in increased electrical conductivity in films due to the difference in crystallite sizes compared to unannealed films. The annealing temperature is associated with the decline in resistivity and film thickness of Cu_2Sb_2O. This film could be a valuable resource for enhancing solar cell efficiency. Copper antimony oxide (Cu_2Sb_2O) exhibits a resistivity that is highly suitable for use as buffer layers in photovoltaic systems.

Table 2. Electrical Parameters of Cu_2Sb_2O

Films	t, (nm)	ρ, (Ω.cm) x 10^7	σ, (S/m) x 10^5
Cu_2Sb_2O	117.53	25.77	3.88
Cu_2Sb_2O 200 °C	114.24	23.45	4.26
Cu_2Sb_2O 300 °C	105.45	16.81	5.94
Cu_2Sb_2O 400 °C	105.31	16.62	6.01

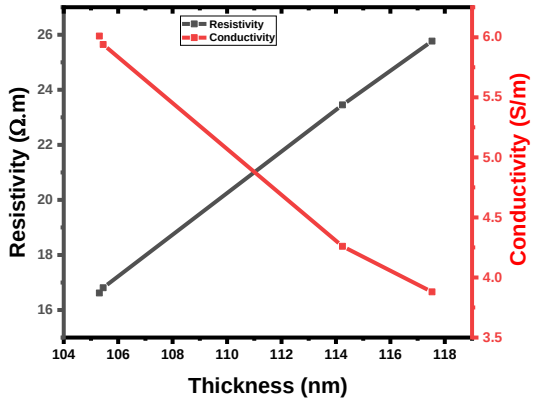

Figure 7. resistivity and conductivity against thickness.

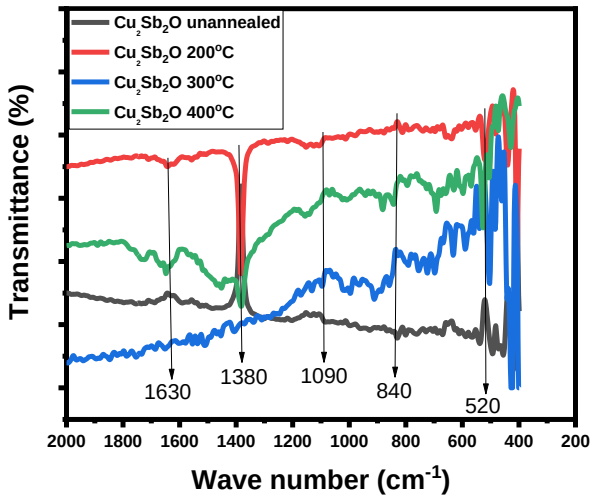

Figure 8. IR spectra of Cu_2Sb_2O.

The IR spectra of Cu_2Sb_2O

The FTIR spectra of Cu_2Sb_2O ranges from 400 cm^{-1} to 2000 cm^{-1} wave number. Cu^{2+} ions are detectable in the films upon increasing the annealing temperature, resulting in the appearance of a symmetrical peak at 840 cm^{-1}, which can be attributed to O-H bound to antimony. In all films, a similar pattern is observed where the 840 cm^{-1} band in the asymmetrically stretched carbonates ion at 1380 cm^{-1} decreases with increasing concentration. The band around 1630 cm^{-1} in the spectra is caused by atmospheric CO_2. An absorption peak around 520 cm^{-1} marks the Sb-O stretching vibrations in Cu_2Sb_2O A slight increase in Cu ions causes the band to grow gradually and become sharper. The material experienced this due to a rise in unit cell volume. The strong absorption band observed at around 520 cm^{-1} is thought to be due to the bending vibration of the Oxygen octahedral deformation mode.

Conclusions

The hydrothermal technique was used to synthesize Cu_2Sb_2O successfully. The pattern shows Cu_2Sb_2O in an irregular phase before annealing and in a polycrystalline phase after annealing at different temperatures between 200 and 400 ˚C. The diffraction peaks (111), (211), and (311) correspond to 2theta angles of 26.934º, 34.228º, and 38.362º respectively. The film's lattice reformed and crystallized because of high annealing temperature, which may cause cell ignition. The peaks were shifted to higher diffraction angles, because of the assumption that the annealing process caused an effect on the material. Small nanoparticles and a significant nanoflake structure are evident in the unannealed Cu_2Sb_2O material. The size of the nanoparticle increases when the film surface is ignited with higher pressure upon annealing at different temperatures. The presence of nanoparticle clusters during annealing resulted in an increase in the material's surface energy. Absorption spectra maintained a high rate of absorption from 200 to 600 nm but decreased significantly beyond that point, with the lowest point at 700 to 850 nm. However, it rose once more during the wavelength range of 980 to 1100 nm. Cu_2Sb_2O has a high capacity for absorbing light, especially in the ultraviolet and blue regions. Annealing Cu_2Sb_2O at 200 ˚C improved the film's absorbance from 0.145 to 0.185 a.u. Raising the temperature from 200 to 400ºC improved Cu_2Sb_2O's absorbance due to its sensitivity to temperature. The films were found to have low reflectance in both regions, making them highly suitable for use in both solar and photovoltaic cells. The bandgap energy of the synthesized Cu_2Sb_2O film decreased from 1.78 eV to a range of 1.66–1.21 eV as the annealing temperature increased from 200 to 400 °C.

Disclosure of conflicting interest

The authors declare that they have no personal or financial conflicts that could have influenced the research described in this paper.

Availability of data

Upon request, data is available.

Orcid

Imosobomeh L. Ikhioya: 0000-0002-5959-4427

References

[1] D. Aldakov, A. Lefrançois, P. Reiss, *J. Mater. Chem. C,* **2013**, *1*, 3756–3776. [CrossRef], [Google Scholar], [Publisher]

[2] I. El Radaf, M. AlKhalifah, M. El-Bana, *J. Non. Cryst. Solids,* **2022**, *588*, 121612. [CrossRef], [Google Scholar], [Publisher]

[3] J.M. Mosby, A.L. Prieto, *J. Am. Chem. Soc.,* **2008**, *130*, 10656–10661. [CrossRef], [Google Scholar], [Publisher]

[4] P.B. Patil, S.S. Mali, V.V. Kondalkar, N.B. Pawar, K.V. Khot, C.K. Hong, P.S. Patil, P.N.

Bhosale, *RSC Adv.*, **2014**, *4*, 47278–47286. [CrossRef], [Google Scholar], [Publisher]

[5] A.J. Perez, A. Vasylenko, T.W. Surta, H. Niu, L.M. Daniels, L.J. Hardwick, M.S. Dyer, J.B. Claridge, M.J. Rosseinsky, *Inorg. Chem.*, **2021**, *60*, 19022–19034. [CrossRef], [Google Scholar], [Publisher]

[6] A. Rabhi, M. Kanzari, B. Rezig, *Thin Solid Films*, **2009**, *517*, 2477–2480. [CrossRef], [Google Scholar], [Publisher]

[7] G.Y. Senguler, E.K. Narin, S.B. Lisesivdin, T. Serin, *Phys. B Condens. Matter*, **2023**, *648*, 414424. [CrossRef], [Google Scholar], [Publisher]

[8] R.S. Marquina, T. Sanchez, E. Regalado-Perez, J. Pantoja-Enriquez, N. Mathews, O.S. Martinez, X. Mathew, *Vacuum*, **2022**, *204*, 111355. [CrossRef], [Google Scholar], [Publisher]

[9] S.Y. Tee, D. Ponsford, C.L. Lay, X. Wang, X. Wang, D.C.J. Neo, T. Wu, W. Thitsartarn, J.C.C. Yeo, G. Guan, *Adv. Sci.*, **2022**, *9*, 2204624. [CrossRef], [Google Scholar], [Publisher]

[10] M. Wu, S. Yu, L. He, L. Yang, *J. Mater. Sci. Mater. Electron.*, **2016**, *27*, 12604–12609. [CrossRef], [Google Scholar], [Publisher]

[11] L. Zhou, E. Bainglass, M. Masroor, B. Giri, G. Li, A. Carl, R.L. Grimm, M.N. Huda, L.V. Titova, P.M. Rao, *J. Mater. Chem. A*, **2021**, *9*, 1643–1654. [CrossRef], [Google Scholar], [Publisher]

[12] E. Bainglass, M.N. Huda, *J. Electrochem. Soc.*, **2019**, *166*, H3195. [CrossRef], [Google Scholar], [Publisher]

[13] M.M. Alkhamisi, A.F. Qasrawi, H.K. Khanfar, *Cryst. Res. Technol.*, **2023**, *58*, 2300049. [CrossRef], [Google Scholar], [Publisher]

[14] S.P. Berglund, F.F. Abdi, P. Bogdanoff, A. Chemseddine, D. Friedrich, R. van de Krol, *Chem. Mater.*, **2016**, *28*, 4231–4242. [CrossRef], [Google Scholar], [Publisher]

[15] N. Chaglabou, M. Kanzari, **2013**, 2, 4195–4201. [Google Scholar], [Publisher]

[16] P. Chongngam, E. Wongrat, A. Tubtimtae, *Optik (Stuttg).*, **2023**, *288*, 171194. [CrossRef], [Google Scholar], [Publisher]

[17] S.E. Mousavi Ghahfarokhi, K. Helfi, M. Zargar Shoushtari, *Adv. J. Chem. A*, **2022**, *5*, 45–58. [CrossRef], [Publisher]

[18] F.Z. Krimech, S. Sayouri, *Mater. Today Proc.*, **2020**, *30*, 909–917. [CrossRef], [Google Scholar], [Publisher]

[19] S. Althobaiti, M. Alghamdi, B. Alamri, A. Madani, *Optik (Stuttg).*, **2023**, *275*, 170534. [CrossRef], [Google Scholar], [Publisher]

[20] I.L. Ikhioya, C.O. Ugwuoke, F.U. Ochai-Ejeh, *Mater. Res. Innov.*, **2023**, 1–8. [CrossRef], [Google Scholar], [Publisher]

[21] I.L. Ikhioya, A.C. Nkele, *Results Opt.*, **2023**, *12*, 100494. [CrossRef], [Google Scholar], [Publisher]

[22] I.L. Ikhioya, F.U. Ochai-Ejeh, C.I. Uruwah, *Mater. Res. Innov.*, **2023**, 1–10. [CrossRef], [Google Scholar], [Publisher]

[23] F. Ali, S. Fazal, N. Iqbal, A. Zia, F. Ahmad, *J. Med. Nanomater. Chem.*, **2023**, *5*, 106–124. [CrossRef], [Publisher]

[24] I.L. Ikhioya, A.C. Nkele, D.N. Okoli, *Optik (Stuttg).*, **2022**, *260*, 169055. [CrossRef], [Google Scholar], [Publisher]

[25] I.L. Ikhioya, A.C. Nkele, D. Okoli, A. Ekpunobi, I. Ahmed, *J. Indian Chem. Soc.*, **2022**, *99*, 100641. [CrossRef], [Google Scholar], [Publisher]

[26] A.I. Agbrara, E.O. Ojegu, M.O. Osiele, I. Ikhioya, *Adv. J. Chem. A*, **2023**, *6*, 401–411. [CrossRef], [Google Scholar], [Publisher]

[27] P. Badr, M. Sajjadnejad, S.M. Haghshenas, *Prog. Chem. Biochem. Res.*, **2023**, *6*, 292–313. [CrossRef], [Publisher]

[28] I.L. Ikhioya, S.O. Aisida, I. Ahmad, F.I. Ezema, *Chem. Phys. Impact*, **2023**, *7*, 100269. [CrossRef], [Google Scholar], [Publisher]

[29] A. Johnson, *J. Eng. Ind. Res.*, **2023**, *4*, 93–109. [CrossRef], [Publisher]

[30] A. Heidaripour, F. Salmani, T. Barati, *Asian J. Green Chem.*, **2023**, *7*, 140–148. [CrossRef], [Publisher]

[31] I.L. Ikhioya, C.O. Ugwuoke, R.M. Obodo, D. Okoli, C.U. Eze, M. Maaza, F.I. Ezema, *Appl.*

Surf. Sci. Adv., **2022**, *9*, 100232. [CrossRef], [Google Scholar], [Publisher]

[32] K.I. Udofia, I. Ikhioya, D.N. Okoli, A.J. Ekpunobi, *J. Med. Nanomater. Chem.*, **2023**, *5*, 135–147. [CrossRef], [Publisher]

[33] I.L. Ikhioya, E.U. Onoh, D.N. Okoli, A.J. Ekpunobi, *Mater. Res. Innov.*, **2023**, 1–9. [CrossRef], [Google Scholar], [Publisher]

[34] Amos, P., Louis, H., Adesina Adegoke, K., Eno, E. A., Udochukwu, A. O., Odey Magub, T. *J. Med. Nanomater. Chem.*, **2022**, *4*, 252–239. [Publisher]

[35] N. Iqbal, S. Khan, F. Ahmad, *J. Med. Nanomater. Chem.*, **2023**, *5*, 186–198. [CrossRef], [Publisher]

HOW TO CITE THIS ARTICLE

Imtiaz Ahmad, Javaria Razzaq, Ammara Ammara, Ferhan Kaleem, Muhammad Qamar, Shahid Ilahi, Imosobomeh L. Ikhioya. Impact of Annealing Temperature on Hydrothermally Synthesized Copper Antimony Oxide (Cu_2Sb_2O) from Amorphous Phase to Monoclinic Structure. *Adv. J. Chem. A*, 2024, 7(2), 110-121.

DOI: 10.48309/ajca.2024.419363.1429
URL: https://www.ajchem-a.com/article_183118.html